INSTITUTE OF PHYSICS PUBLISHING MEASUREMENT SCIENCE AND TECHNOLOGY

Meas. Sci. Technol. **17** (2006) 2367–2379 doi:10.1088/0957-0233/17/9/001

Wavelet packet denoising for online partial discharge detection in cables and its application to experimental field results

A Kyprianou[1], P L Lewin[2], V Efthimiou[3], A Stavrou[3] and G E Georghiou[2,4]

[1] Department of Mechanical and Manufacturing Engineering, School of Engineering, University of Cyprus, PO Box 20537, Nicosia 1678, Cyprus
[2] The Tony Davies High Voltage Laboratory, School of Electronics and Computer Science, University of Southampton, Southampton, SO17 1BJ, UK
[3] Electricity Authority of Cyprus, PO Box 24506, Nicosia 1399, Cyprus
[4] Department of Electrical and Computer Engineering, School of Engineering, University of Cyprus, PO 20537, Nicosia 1678, Cyprus

E-mail: akyp@ucy.ac.cy

Received 7 April 2006, in final form 20 June 2006
Published 24 July 2006
Online at stacks.iop.org/MST/17/2367

Abstract
Partial discharge measurements taken online are severely corrupted by noise due to external disturbances. In this paper a powerful noise reduction technique, based on a wavelet packet denoising algorithm, is employed to isolate the signals from the noise. This methodology enables the denoising of partial discharges that are heavily corrupted by noise without assuming any *a priori* knowledge about the partial discharge features. A brief description of the wavelet packet theory as an extension of the multi-resolution analysis is given. Results of the application of this algorithm to simulated data of low signal-to-noise ratio are presented, demonstrating substantial improvement in signal recovery with minimum shape distortion. Finally, the capability of this technique is highlighted by applying it to experimental field data taken from three-phase 11 kV cables.

Keywords: partial discharges, partial discharge detection, wavelet packets, noise rejection, field measurements, cables

(Some figures in this article are in colour only in the electronic version)

1. Introduction

Ensuring reliable and uninterrupted operation of transmission and distribution networks poses a key challenge in the area of monitoring and maintenance of power engineering systems. Indeed, monitoring the condition of high-voltage (HV) systems and cable networks is becoming increasingly important as customers demand cheaper electricity with greater security of supply. In turn, this translates to increased loading of HV cable circuits, whilst reducing overall maintenance and repair costs. Moreover, with unscheduled shutdown of equipment, additional costs are often incurred, which are subsequently found to be significantly above the cost of necessary repairs. A satisfactory online method of anticipating failure of key components is therefore required, so as to attain an economic lifetime extension of high-voltage equipment.

In determining system reliability, the role of partial discharge (PD) is paramount, as it is a serious degradation stress mechanism, the precursor of insulation failure and a symptom of ageing occurring [1, 2]. A schematic diagram of a typical system for online PD condition monitoring is shown in figure 1. Initially, test system calibration has to be undertaken followed by data acquisition. The process of data acquisition essentially consists of the PD sensing stage, which can be achieved either electrically, acoustically, optically, chemically

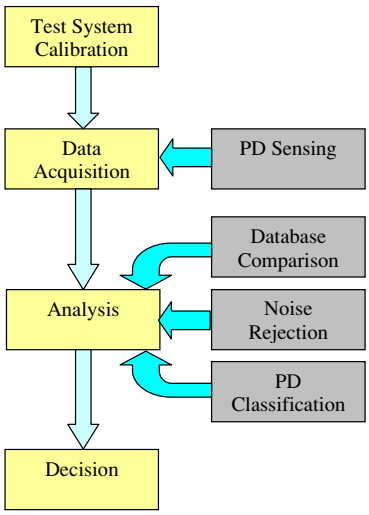

Figure 1. Condition assessment system.

or by a combination of these approaches. Following sensing, the analysis of the measured data is necessary. Noise rejection, PD database comparison and PD classification methods have been proposed and are required before reaching a decision on the integrity of the system and any subsequent action that needs to be taken.

PDs are evident inside HV assets as a result of such defects as insulation impurities or ageing due to thermal, mechanical and electrical stresses. Much effort has been focused on unveiling the actual mechanisms that cause cable deterioration. To this end, Morshuis used the method of time resolved measurements to relate the PDs in voids to dielectric degradation [3] as well as to simulate the ageing processes that void discharges cause [4]. Mayoux *et al* [5] demonstrated the possibility of occurrence of pre-PD microdischarges in the microstructure of the insulation material and have also shown that void gas pressure, diffusion solubility, crystalline fraction of the polymer of which the insulation is made and the temperature gradient, affect the initiation and propagation of PDs. This pointed to the need for more detailed analysis of the cable microstructure. Avila *et al* [6] reported image testing of cables, under various conditions, using conventional ultrasound, acoustic, optical and scanning electron microscopy. Through this study they established the correlation between the void density and size in the cable material and its life span. As a high percentage of failures are associated with PD, its testing, therefore, provides relevant information on the integrity of an electrical system.

Techniques for detecting and locating PDs have been the subject of research since the 1920s [7]. Work in this area mainly focused on developing techniques for systematic classification of PDs through various statistical indices [8] and pattern analysis [9]. Heitz [10] derived a physical model of PD relying on the probabilistic nature of the PD events and demonstrated that it is possible to correlate the model parameters with the PD phase resolved patterns. Alterburger *et al* [11] extended the work of Heitz by implementing a maximum likelihood method for estimating the stochastic model parameters on simulated and experimental PD phase resolved patterns. Wu *et al* [12] have also studied the pattern of PD phases with respect to discharge area variation. Their analysis showed that for each PD pulse there exists a constant probability for inducing another such pulse which in turn creates certain statistical patterns and hence allows classification and decision making.

The sensor technology utilized to measure PDs relies on the electrical, acoustic, optical and chemical consequences of PD activity in the insulation [13]. Oyegoke *et al* have published a survey on the actual sensor hardware developed that utilizes each of the above phenomena [14]. For non-conventional electrical detection methods then the issue of calibration is receiving attention, because of the possibilities of including capacitive coupler sensors within the design of high-voltage accessories [15].

The focus of the paper is the development of a powerful noise reduction technique which can isolate the signals from the noise following online PD detection. The technique is based on a wavelet packet denoising algorithm which allows heavily corrupted signals to be denoised without assuming any *a priori* knowledge about the PD features. Results of the application of the algorithm to simulated data of low signal-to-noise ratio are presented, demonstrating substantial improvement in signal recovery with minimum shape distortion. Finally, the capability of this technique is highlighted by applying it to experimental field data taken from three-phase 11 kV cables.

The following section discusses thoroughly the literature pertaining to denoising of PD using wavelets and wavelet packets. The discussion unveils the knowledge gap that the work of this paper fills. Section 3 provides a description of wavelet packets as an extension of multi-resolution analysis. In section 4, the results of applying the algorithm to various cases of simulated PD signal data corrupted by white noise are presented. Finally, in section 5 the algorithm is applied to field data obtained from three 11 kV underground cables belonging to the network of the Electricity Authority of Cyprus (EAC) demonstrating the ability of the algorithm to reject the noise of the field data with minimal distortion.

2. Wavelets and wavelet packets for PD denoising: previous work

Generally, conventional digital signal processing techniques are not capable of detecting low-level PD activity in environments where there are significant levels of noise [16]. Towards the alleviation of this problem and in conjunction with the more general awareness of the specific abilities of the wavelet transform, research has been undertaken to employ denoising algorithms based on the wavelet transform [17]. Wavelet transforms have become popular in other areas of damage detection and feature selection due to their proven advantages, namely adaptability and high-resolution simultaneous frequency- and time-domain analysis [18, 19]. Below we outline the relevant work carried out in the context of wavelet and wavelet packet denoising of PDs.

2.1. Wavelets

Shim *et al* [20] gave one of the earliest discussions of the application of wavelet-based denoising techniques to PDs. In

this paper, they overviewed the digital processing techniques that had been applied in detecting PDs. After discussing, in the context of PD, the fact that the ability to separate signal from noise improves with increased knowledge of the signal source, they undertook a survey of the signal processing methods applied to PD denoising, namely, averaging, autocorrelation, higher order statistics, adaptive filters, fractal analysis and neural networks. The authors then went on to discuss the various sources of noise in PD measurements and to survey closed and open loop noise reduction techniques. They finally presented results of denoising a single PD trace using wavelets without giving the exact methodology of achieving this. This methodology is described in [21] where Shim *et al* also presented the theoretical multi-resolution analysis and thresholding which are the main ingredients of the wavelet denoising scheme. They denoised PDs on a 33 kV, 1.3 m long oil-impregnated paper three-conductor cable, with data acquired after PD triggering using hard thresholding and Daubechies 2 wavelet. Their main conclusion was that the effectiveness of the denoising relied on the thresholding values and the number of decomposition levels. They concluded by suggesting that this scheme could improve by developing numerical methodologies for automatic threshold and wavelet selection. In a subsequent paper, Shim *et al* [22] applied their methodology to denoise and locate PD injected in 11 kV and 33 kV cables online. In this study the authors used the Daubechies 9 wavelet and decomposed the signal up to six levels.

Boggs *et al* [16] in their study of the fundamentals of PDs, in the context of field cable testing concluded that the available digital signal processing techniques up to the time of the work presented in this publication were insufficient for online PD detection and required PD trigger above the noise. This rendered the techniques unable to detect PDs buried in noise, lowering the probability of successfully estimating system failures.

In the endeavours to alleviate the problems highlighted above and to provide a more systematic way of applying wavelet-based denoising to PDs, Ma *et al* [23] touched on the following related issues: wavelet patterns of PD shapes taken from typical RC and RLC PD detecting circuits, types of noise corrupting PDs and methodologies for automated selection of optimal threshold and wavelet selection. In particular, they decomposed the PDs obtained from the detecting circuits on orthogonal bases constructed from Daubechies 2 and Daubechies 8 wavelets. On the same bases, they also decomposed the types of noise they considered, namely, white and narrow-band noise. They went on to utilize the information they extracted from these decompositions by devising a denoising scheme where the number of decomposition levels required is chosen by observing the levels in which the PD coefficients are mostly clustered. In another publication Ma *et al* [24] applied this methodology to different results.

Satish *et al* [25] presented a comparison between the wavelet-based denoising methodology and the conventional methods of FIR and IIR filtering. They concluded that the wavelet-based method was able to remove all three types of noise they considered simultaneously with minimum distortion, as opposed to the other methods. In an attempt to improve the effectiveness of the wavelet-based PD denoising, Zhou *et al* [26] presented further analysis on how the structure of the conjugated mirror filters associated with multi-resolution analysis relates to the PDs. Utilizing this knowledge they presented an improved methodology in denoising PDs using the wavelet transform.

Wavelet analysis has been used in other areas of partial discharge analysis such as in classification of multisource PD patterns [27] and in detecting electromagnetic [28] and acoustic [29] signals emitting due to PD occurrence.

It has so far been demonstrated that PD denoising using wavelets is possible but this can be achieved only when (a) there exists prior knowledge of signal characteristics (this is due to the short time bandwidth of the real PDs) and (b) the PD triggers above the noise level. Consequently, the above methodologies cannot denoise PDs that are (a) well buried in noise, i.e. their peak value is either of the same order of magnitude or lower than the standard deviation of the noise and (b) obtained from measurements on actual in service field cables.

2.2. Wavelet packets

A new method based on wavelets that could denoise PDs by alleviating the above shortcoming is a scheme that relies on wavelet packets. The theory of wavelet packets is briefly explained in the paper as an extension to multi-resolution analysis, the backbone of the wavelet-based denoising technique described earlier.

Chang *et al* [30] applied this methodology to denoise known PDs taken from GIS stations and artificially corrupted by white noise. Utilizing the prior knowledge of the PDs, they separated them into a training and a test set. They used the training set to establish the optimal wavelet packet, decomposition level and the best tree. They showed that the wavelet symlet 8 and hard thresholding gave better results for denoising. Chang *et al* [31] also used wavelet packets combined with neural networks (NN) in order to separate coronas from PDs. They used various predetermined signals of PDs, coronas and mixtures of them to train the NN. The NN was trained by feature vectors that were created from data obtained from the wavelet packet decomposition of the original signal. Knowing the decomposition of predetermined PDs and coronas then they could utilize the nodes corresponding to the PD in order to reconstruct the PD from a mixed signal.

Wavelet packets have also been used in related areas of power systems such as power system disturbances [32, 33] and energy measurements [34]. This paper features a methodology of denoising and detecting PDs that does not require the existence of any *a priori* knowledge of its characteristics such as its bandwidth and origin of occurrence. The above becomes evident in section 5 that presents the results from field experimental data. In this section, the capability of the algorithm is highlighted by denoising simultaneously short time bandwidth (wide frequency bandwidth) and short frequency bandwidth (wide time bandwidth) field data. This is achieved by dint of the entropy criterion of selecting the best basis from the packet of available bases [35–37], which ensures that the signal energy is minimally spread over the selected basis. Its

ability to give succinct decompositions is also demonstrated showing that the coefficients of the decomposition of a noisy PD are mostly clustered at the time–frequency region of the PD occurrence. This is better appreciated when compared with the decomposition coefficients of the same noisy PD over a standard multi-resolution only basis. The entropy value of such a decomposition is high, implying low-quality reconstruction. Finally, the other novelty of the work described in the paper, which is equally important, is the ability to denoise PDs that do not necessarily trigger above the noise floor.

3. Wavelet packet denoising theory

3.1. PD denoising using wavelets

The adaptive capability of wavelets has led to the development of wavelet denoising algorithms that all have a common structure. Firstly, the signal is decomposed on a wavelet basis by correlating the various dilated and scaled versions of a mother wavelet with the original signal. Secondly, a threshold is applied to the resulting wavelet coefficients and finally the signal is reconstructed using the coefficients that survived the threshold process. The reconstructed signal is an estimation of the original without noise. The algorithm presented in this paper extends the capability of denoising through the use of wavelet packets. The basis availability is enlarged yielding more possibilities of finding better decompositions that concentrate on the important signal features. The best basis is selected according to an entropy criterion that can be interpreted as a measure of the signal energy spread over the basis vectors. This criterion is described in section 3.2

In principle, any denoising algorithm that uses thresholding utilizes the fact that noise energy spreads equally over the basis vectors. This yields, as a consequence, many low-value coefficients, whereas more important signal patterns correlate strongly with a few basis vectors giving a few high-value coefficients. Therefore, it is necessary to use appropriate thresholding to ensure that most of the noise-related vectors do not participate in the reconstruction, ensuring that the noise energy is effectively filtered out of the clean signal estimate.

The attempts to discretize wavelet transforms for fast computation and redundancy elimination led to the development of the multi-resolution analysis which achieves discretization using the minimum possible number of basis vectors by securing orthogonality between them [38]. As it is described below such a basis can be constructed using appropriate functions called scaling and wavelet functions. Multi-resolution analysis became the milestone of wavelet packets and denoising as described in sections 3.2 and 3.3 respectively. The main idea of multi-resolution analysis, as shown in figure 2 for two such levels and expressed by equation (1), is the signal decomposition at different levels of detail through the decomposition of each approximation space Af_j:

$$f = Af_N + Wf_1 + \cdots + Wf_N. \tag{1}$$

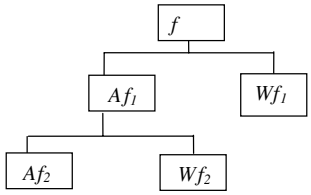

Figure 2. MRA analysis of a signal f up to the second level.

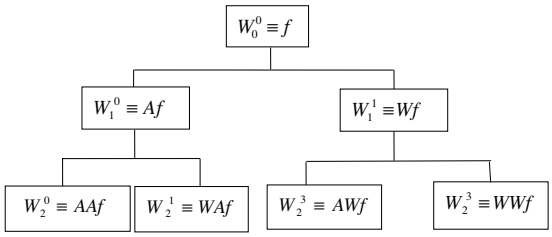

Figure 3. Wavelet packet decomposition of a signal f up to the second level.

3.2. Wavelet packets

A wavelet packet is an extension of the multi-resolution analysis that provides a dictionary D of orthogonal bases [40]. This is achieved not only by decomposing each approximation space Af_j according to equation (1) but also each detail space Wf_j into

$$Wf_j = Wf_{j+1}^a \oplus Wf_{j+1}^b. \tag{2}$$

This decomposition is shown pictorially in figure 3. As can be seen, it provides extra bases on which the signal f can be projected. For example, the following are two possible decompositions of the signal f in spaces extracted from the wavelet packet tree of figure 3:

$$f = Af + AWf + WWf \tag{3a}$$

$$f = AAf + WAf + Wf. \tag{3b}$$

Hence, by using wavelet packets a dictionary of orthonormal bases can be constructed, on which the function can be decomposed and therefore between two different bases there should be a criterion according to which the better basis could be selected. One such criterion is the entropy functional which for a basis of n vectors $\vec{b}_i$ is defined as

$$\varepsilon(\text{basis}) = -\sum_{i=1}^{n} \frac{|\langle f, \vec{b}_i\rangle|^2}{\|f\|^2} \ln\left(\frac{|\langle f, \vec{b}_i\rangle|^2}{\|f\|^2}\right) \tag{4}$$

where $\langle f, \vec{b}_i\rangle$ is the inner product of f with the basis vector $\vec{b}_i$, i.e. the projection of f on $\vec{b}_i$, and $\|f\|$ the norm of the signal f. This criterion, motivated by the communication theory, had been introduced by Coifman *et al* [40] and it measures the signal energy spread over a particular basis. The lower the entropy implies that fewer basis vectors are needed to account for the energy spread so the decomposition is more efficient and the basis better than any other of higher entropy value.

3.3. Denoising algorithm

The denoising algorithm used in this paper is composed of three parts, as already mentioned in section 3.1. The noisy

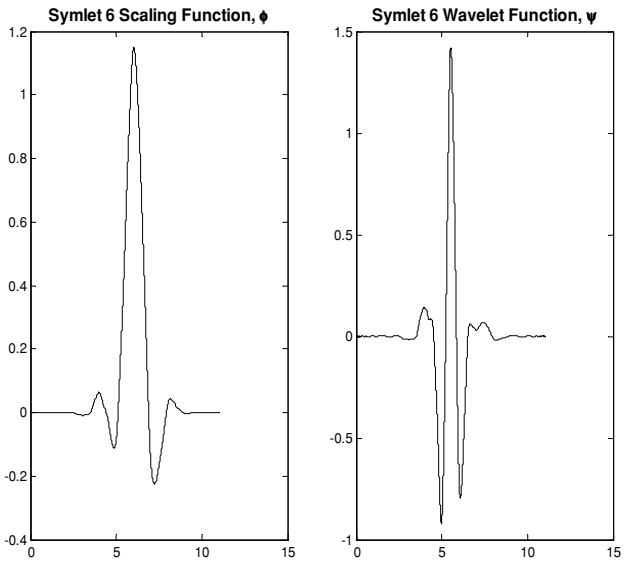

Figure 4. Left: the scaling function of symlet 6; right: the wavelet function of symlet 6.

signal is decomposed on a basis selected from a wavelet packet library of orthogonal bases according to an entropy criterion, then hard thresholding is applied on the decomposition coefficients and finally the signal is reconstructed with the thresholded coefficients. In this section the motivation behind this algorithm is outlined. Further details of its mathematical justification can be found in [41].

If we assume that a signal f is corrupted by an additive white noise ε observed as

$$y = f + \varepsilon, \tag{5}$$

the algorithm should provide an estimate $\hat{f}$ of f from y.

For all the cases studied in this paper, the analysing wavelet used was symlet 6. This wavelet and its associated scaling function are shown in figure 4. Symlet 6 belongs to a family of wavelets that are characterized by the possession of the largest number of vanishing moments for a minimum support and hence it constitutes the best choice for this problem. This means that in the presence of a PD, at a certain scale and translation, the wavelet's or (scaling function's) correlation with the PD would be high, yielding fewer and higher wavelet coefficients. This, in turn, means that the symlet wavelets adapt better to the high-frequency bandwidth of typical PD signals [41].

The symlet family of wavelets is a modified version of the Daubechies wavelets introduced by I Daubechies herself in order to achieve better energy distribution over their support as well as more symmetrical wavelets. Hence all the other Daubechies properties apart from that of symmetry remain intact by the symlet family of wavelets [42].

The traces of the data analysed for this work consisted of $2048 = 2^{11}$ samples. At each decomposition level the signal is down-sampled by a factor of 2. The minimum number of samples that a trace can have in order to be analysed at the lowest decomposition level is $4 = 2^2$. So the number of the decomposition levels that a signal is analysed over is given by $11-3 = 8$, since no analysis can be performed on signals having 2^0 and 2^1 samples. For the work in this paper no

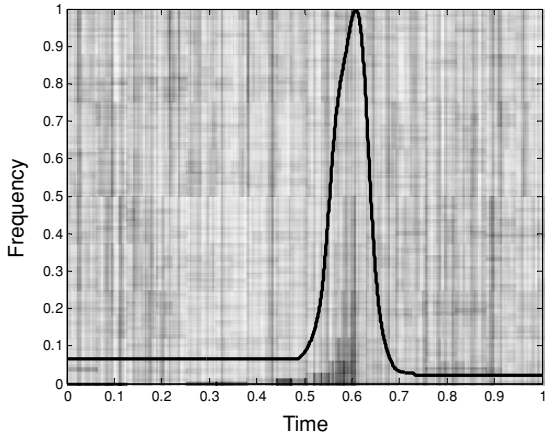

Figure 5. Decomposition of noisy signal on the best basis of wavelet packets.

assumption is made about the PDs and denoising of field data (section 5) was undertaken without any prior assumption about the shape and duration of the PDs.

In order to demonstrate that using wavelet packets yields better results than the usual thresholding wavelet methodology for low SNR PD signals, the following example has been considered. Figure 5 shows the image, on a grey scale plot, of the analysis coefficients on wavelet packet best basis of the noisy signal obtained by corrupting the PD of figure 5 with white noise of standard deviation 75% of the PD peak value. The decomposition of the same signal on the conventional multi-resolution analysis basis is also shown in figure 6. Superimposed on both figures is the uncorrupted PD. In figure 5 the basis coefficients are higher under the PD, as depicted by the darker colour, than in any other area of the phase plane. The uniformity of the major area of the phase plane indicates a noisy signal with the only exception being the small area where the PD occurs. Hence, thresholding these coefficients at a level determined by the noise standard deviation will reject the noise leaving only the coefficients associated with the PD. In contrast, figure 6 indicates that high-value basis coefficients do not occur at the position of the PD.

Taking into consideration that white noise corrupts all wavelet coefficients equally then it could be concluded that large coefficients, in scale and translation, occur at the place where the signal occurs. This calls for thresholding the wavelet coefficients that correspond to the noise.

The last part of the denoising algorithm concerns the choice of thresholding. In this work hard thresholding has been employed. The theory of soft and hard thresholding has been developed in order to get the risk of reconstruction as close as possible to an oracle's optimum risk. This risk, however, is always higher than that of the oracle [41]. The hard threshold removes all the coefficients that have a value less than a threshold level. This level is determined by the noise level as measured by its standard deviation as described in the paper. On the other hand the soft as well as the garotte thresholding decreases all coefficients above a threshold value T and below $-T$ by an amount T. As discussed previously, wavelet packets are used because they provide the best possible basis over which a noisy PD signal can be decomposed. Figure 5 depicts

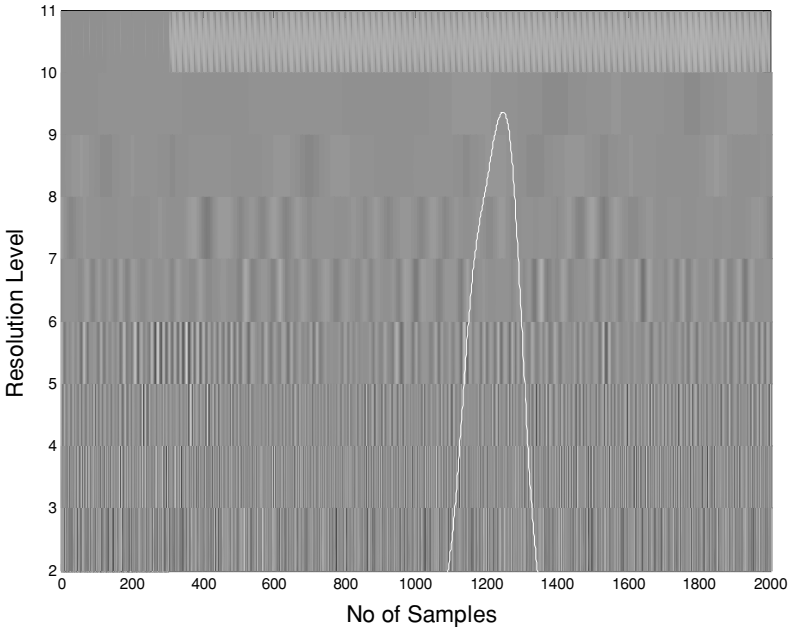

Figure 6. Decomposition of the noisy signal on the basis constructed by MRA.

that all the high-value coefficients cluster around the partial discharge occurrence in the time–frequency plane. Based on this, hard thresholding is the best choice because it will eliminate all the low-level coefficients and will leave the high-value coefficients that represent the signal unchanged.

Hard thresholding trims the low-value coefficients according to

$$\rho_T(w) = \begin{bmatrix} w & \text{if} \quad w > T \\ 0 & \text{if} \quad w \leqslant T. \end{bmatrix} \tag{6}$$

Assuming that y is analysed over the library best basis, say $\{\vec{b}_i^{[\text{best}]}\}_{i=1}^{N}$ then the estimated $\hat{f}$ is given by

$$\hat{f} = \sum_{i=1}^{N} \rho_T(w)\vec{b}_i^{[\text{best}]}. \tag{7}$$

4. Simulated results

The denoising algorithm described in section 2 has been implemented using Wavelab [43] and its effectiveness evaluated through a series of simulation studies. The parameters that dictate the success of this algorithm are the proper selection of the threshold and the mother wavelet. The rationale for selecting the symlet wavelet was explained in the previous section. This algorithm has evolved due to attempts made by mathematical statisticians in extending the Wolfowitz's minimax optimality in estimating the mean of a normal distribution to infinite-dimensional objects such as, for example, one-dimensional (1D) and two-dimensional (2D) signals and densities [41]. Threshold-based wavelet shrinkage, asymptotically in a certain minimax sense, provides the optimal estimator. It has been proved that the threshold value that provides the optimal estimator is given by $T_l = \sigma\sqrt{2\log(n)}$ where σ is the standard deviation of the white noise that contaminates the signal and n is the size of the signal time history [35]. To this end, figure 7 shows the denoising results obtained for different thresholding values on a PD signal corrupted by white noise. The plot of figure 7(*a*) shows the denoising using a threshold value 50% of the corrupted signal standard deviation. The solid line represents the original PD signal while the dotted trace gives the denoised signal. It is obvious that with this low value of threshold coefficients the noise is also retained. This, upon reconstruction, gives a noisy signal with most of the noise still disrupting all the significant features of the buried PD. On the other hand, the plot of figure 7(*b*) which corresponds to a threshold value equal to that of the standard deviation of the noisy signal portrays a very good match between the denoised PD and the original PD. In figure 7(*c*) the threshold value was set to two standard deviations and the matching quality deteriorates significantly. This is due to the fact that the algorithm attenuates wavelet coefficients that correspond to the signal features. Finally, by setting the threshold value to three standard deviations all the signal vanishes since all the analysis coefficients vanish. Subsequently, for the field data analysis and for comparison reasons two threshold values were employed. One of these is set to the threshold value equivalent to 50% of the noisy field signal's standard deviation and the other to a value equivalent to a single standard deviation of the noisy field signal.

The simulation below has used single pulse signals corrupted with different levels of white noise to determine the minimum signal-to-noise ratio and pulse duration that still allow effective denoising. Table 1 details the range of tests undertaken.

Typical results for a 5 ns pulse buried in white noise with a standard deviation of 125% of the peak pulse voltage are shown in figure 8. The output of the denoising algorithm when compared to the original pulse is in good agreement (figure 8(*b*)) and has a peak value of 22.8 mV which is equivalent to 94.5% of the original. At this point, it is important to note that the choice of the peak absolute value

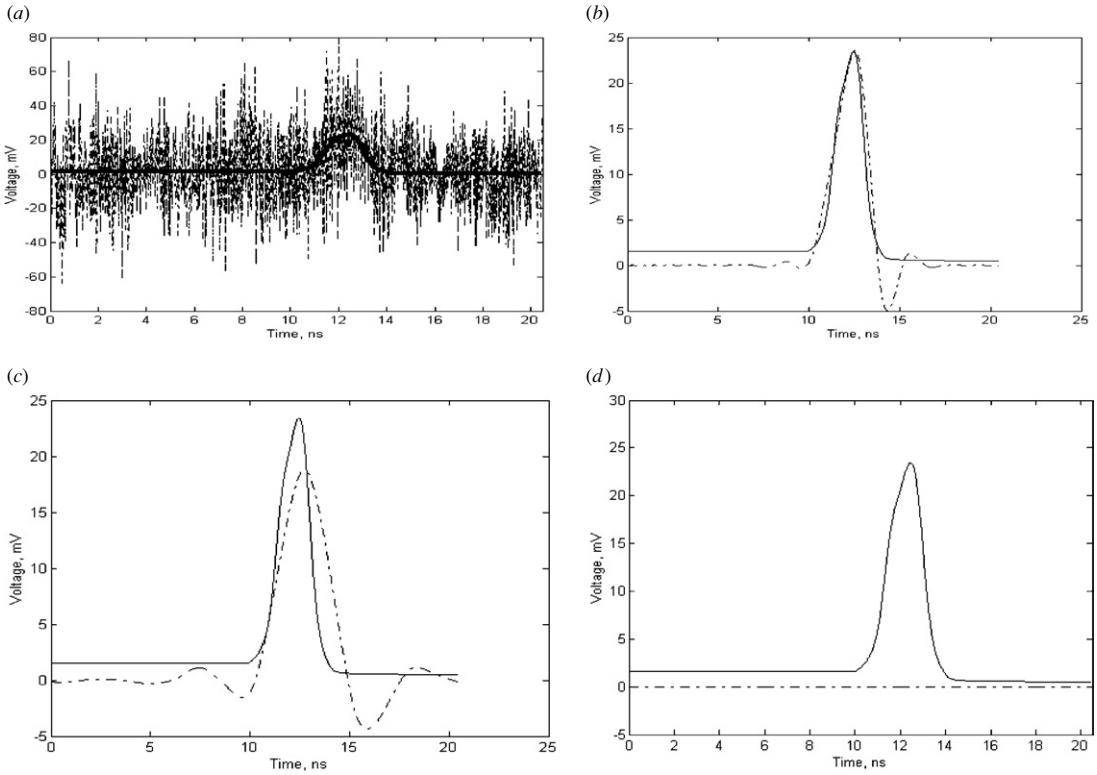

Figure 7. Denoised signal with threshold value set to (*a*) 0.5σ, (*b*) 1σ, (*c*) 2σ and (*d*) 3σ. Solid line: original signal. Dashed line: denoised signal.

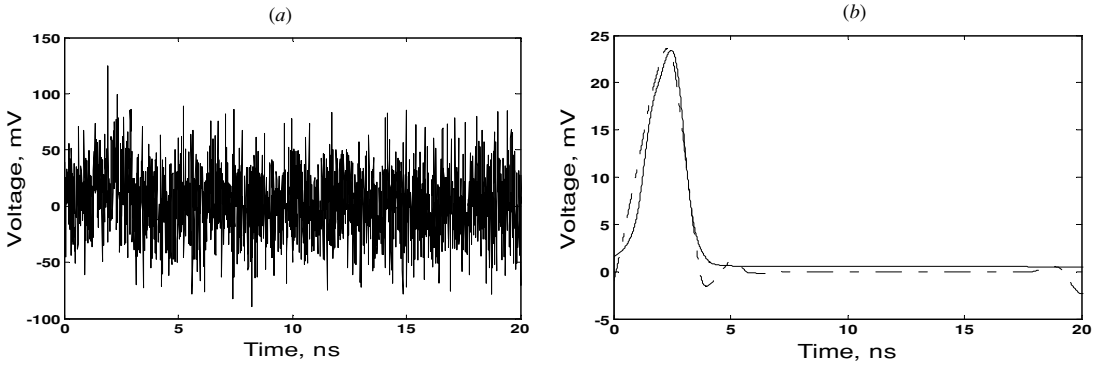

Figure 8. Simulation of 5 ns single pulse buried in white noise ($\sigma = 28.125$ mV): (*a*) input signal to denoising algorithm, (*b*) comparison of original and denoised signal. Solid line: original signal; dashed line: denoised signal.

Table 1. Simulation variables and pulse detection reliability.

Pulse duration (ns)	Peak pulse voltage (mV)	White noise standard deviation (mV)	Detection reliability
10	23.5	16.875	100
10	23.5	28.125	100
5	23.5	16.875	100
5	23.5	28.125	100
1	23.5	16.875	60
1	23.5	28.125	60

of the simulated PD pulse, which is about 23.5 mV for this particular signal, has no significance as the important parameter is the signal-to-noise ratio (SNR). For practical PD measurements, it is important that any denoising filter does not substantially attenuate the signal peak values as these are indicative of the magnitude of a detected PD event. Reliable detection of single pulse events with duration of 5 ns would indicate that PD signals with a bandwidth of 100 MHz can be effectively denoised using this method.

To further investigate the effect of measurement signal bandwidth on the performance of the algorithm, analysis of single pulses having duration of 1 ns was undertaken. In practical terms, such signals are unlikely to be produced using VHF sensing techniques due to the bandwidth of the sensor (typically 200–250 MHz maximum). A typical result where the denoising algorithm recognized the presence of a single pulse is shown in figure 9. Over a series of trials the algorithm preserved the original pulse 60% of the time. The reduction in detection reliability is because for such low time duration

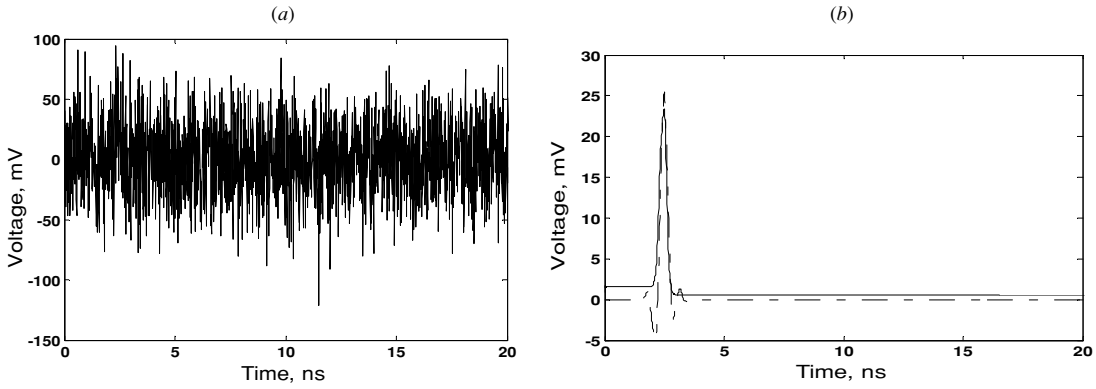

Figure 9. Simulation of 1 ns single pulse buried in white noise ($\sigma = 28.125$ mV): (*a*) input signal to denoising algorithm, (*b*) comparison of original and denoised signal. Solid line: original signal; dashed line: denoised signal.

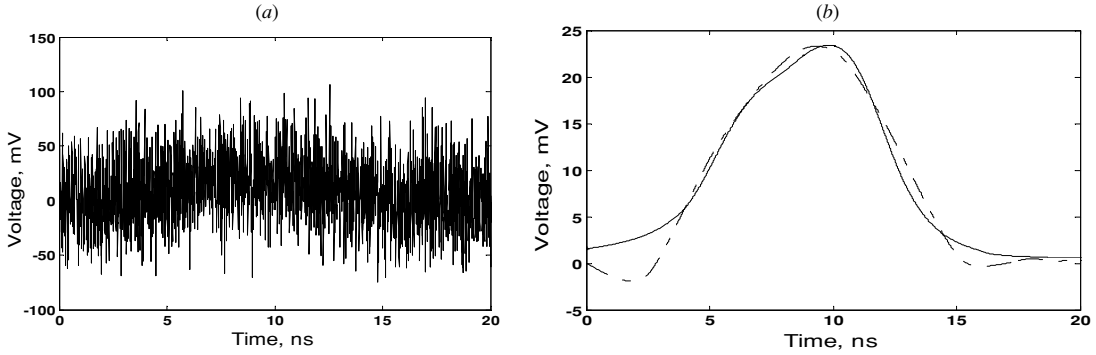

Figure 10. Simulation of 10 ns single pulse buried in white noise ($\sigma = 28.125$ mV): (*a*) input signal to denoising algorithm, (*b*) comparison of original and denoised signal. Solid line: original signal; dashed line: denoised signal.

pulses buried in high levels of noise, the pulse can be assumed to be an artefact of the noise and falsely rejected.

Another aspect of this algorithm is that there is minimal pulse shape distortion which is of paramount importance for condition monitoring applications where analysis of pulse shape can provide information with regard to source location or identity of the type of PD activity. Figure 10 shows a comparison between an original 10 ns single pulse and the denoised signal demonstrating this. In contrast to conventional filtering methods, where there is convolution between the input signal and the filter impulse response, the technique presented here uses a different approach by decomposing the signal over a basis and proceeding by rejecting basis vectors according to a measure of the energy spread over these vectors. In other words, each basis vector corresponds to a pattern that correlates to a certain degree with various signal features.

The simulation studies have provided confidence in this approach and it has subsequently been applied to data obtained from 11 kV underground cable circuits of the Electricity Authority of Cyprus (EAC).

5. Experimental field results

A large number of EAC underground cable circuits has been monitored over a period of several months in order to obtain data with respect to the presence of PD, cable deterioration and ultimate failure. From this data set, three different cases are considered here to demonstrate the denoising algorithm. Future work will concentrate on the development of classification schemes based on the analysis of denoised data.

The length range of cable considered for this work varies from 50 m to around 800 m and there are joints at about every 200–300 m. The experimental measurements were obtained by inductive coupling measurements made at the terminations of three EAC substations. It is important to emphasize that the PDs we measure are essentially the PDs that are obtained at the terminations and the ground connection lead. The cables under test were 11 kV three-phase paper impregnated, non-draining insulated with 120 mm^2 shaped stranded conductor, lead covered, double steel taped armour and PVC oversheath. They were situated in plastic pipes of 110 mm diameter, buried in the ground at a depth of 1.1 m, close to distribution substations. These cables are joined either to other paper insulated or to XLPE rated 11 kV or 22 kV cables using cast iron compound field and heat shrinkable joints. The sampling rate of the data acquisition is 18 kHz. The data are stored in text files of typical size around 10 Mb for every 1 min of measurement.

The test equipment consists of a commercially available differential probe (LDP 5) which is attached to an inductive sensor that is applied to the ground connection lead. Any PD processes which appear inside the system are traceable even on grounded parts because of the very high-frequency components of PD transients up to several tens and hundreds of MHz. The magnetic field around the ground connection caused by the high-frequency currents induces a voltage in the winding of the inductive sensor and this voltage is measured.

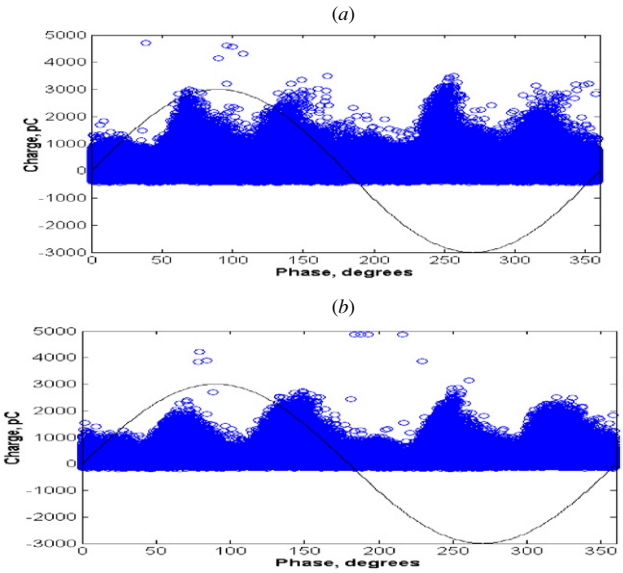

Figure 11. Cable 1; PD against phase: (*a*) first measurement, 2785 cycles, (*b*) second measurement taken two months after the first, 2819 cycles.

This offers the advantage that no connection to the high voltage is required and hence can be used while the test object is in service. Furthermore, no coupling capacitors are required. The signal from the sensor is then digitized (through an analogue to digital converter card) and recorded on the hard disk of a laptop computer. This allows PD events to be recorded with respect to magnitude, time and phase angle. The interpretation of the results is based mainly on the evaluation of trends in the PD level development and hence relative measurements are of interest. Comparison of previously recorded data sets therefore allows trending to be observed.

The calibration of the inductive sensor has been performed according to the manufacturer's recommendation. The earth connection lead is simulated by a wire having a length of 200 mm and a width of 150 mm. The input terminals of the wire loop are connected to the charge injector, whereas the sensor is fixed to the opposite part. The arrangement must be positioned in such a way that the area of the calibrating wire loop coincides with the area of the sensor. It has to be stressed, however, that on the basis of the above calibration procedure, the data obtained from the field results are not identical to the apparent charge of the PD, determined in standard PD measuring circuits. Rather, the main purpose of the above calibration is to ensure reproducible results, which is important with respect to repeated PD tests. Furthermore, every effort has to be made so that the same coupling factor by the inductive sensor is achieved in order to allow comparison of the different results.

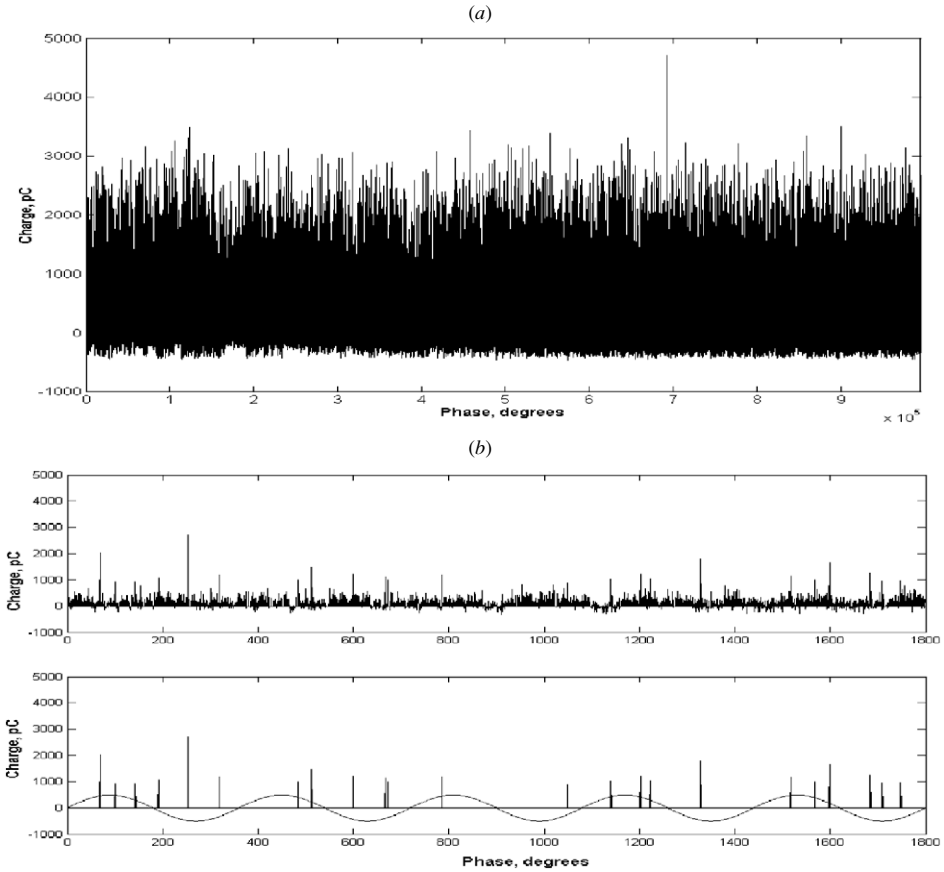

Figure 12. Cable 1: (*a*) first measurement raw data; (*b*) subset of denoised data, threshold equal to $\sigma/2$ and σ.

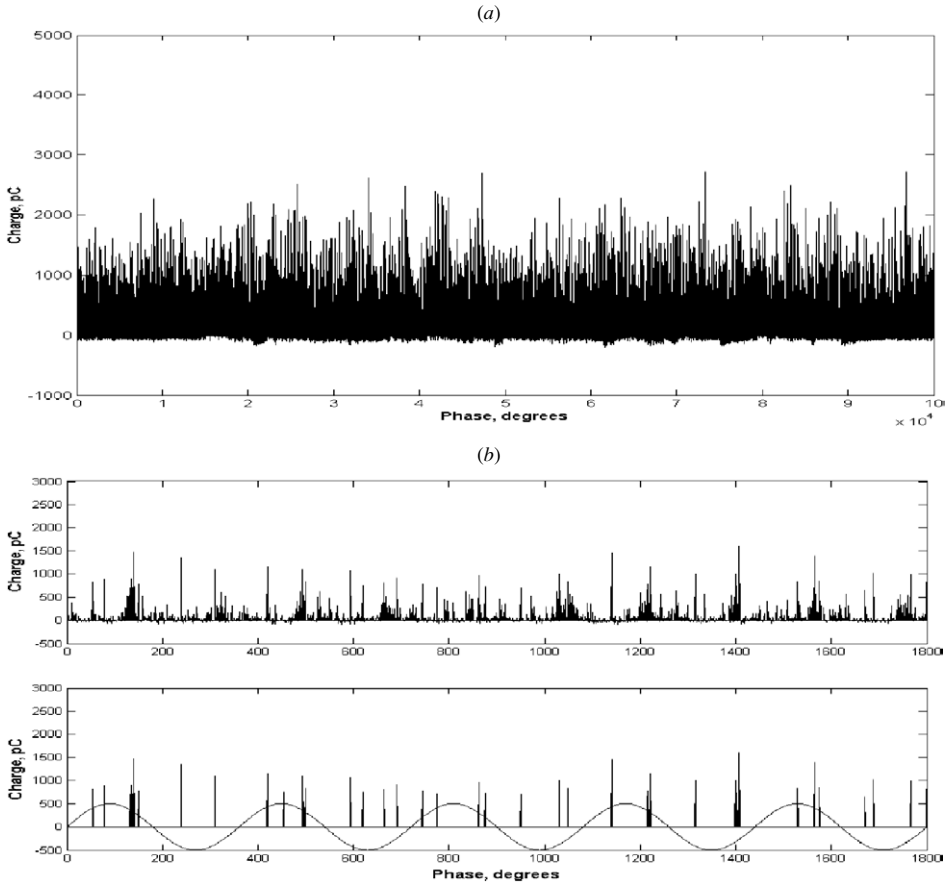

Figure 13. Cable 1: (*a*) second measurement raw data; (*b*) subset of denoised data, threshold equal to $\sigma/2$ and σ.

The primary aim of this study is to assess the capability of the wavelet packet algorithm to denoise effectively the field results. This has been achieved by studying the time-domain measurement signals from the three cables in order to elucidate and resolve the role of PD and correlate it with the event of insulation failure.

5.1. Cable 1: continuous high PD activity without resulting in insulation failure

Figure 11 shows two non-denoised phase plots of the measured PD signal, where the second measurement was made two months after the first one. Superimposed on the phase plots is a sine wave of arbitrary amplitude in order to demonstrate the relationship between the phase of the applied voltage on the cable and the discharge occurrence. Initial interpretation of the phase plots is that they are indicative of high PD activity with high subjective failure expectation. However, to date cable 1 has not failed and at the time of writing is still in normal operation.

To analyse these data, they were firstly subdivided into contiguous windows of 2048 values and then each window of raw data was analysed sequentially. As has already been discussed from the results of the simulation study, two threshold values were set to $\sigma/2$ and σ of the noisy data. Figures 12 and 13 show the raw data and denoised signals obtained for the two measurements of cable 1, clearly the higher the threshold the fewer PD events that are clearly detected.

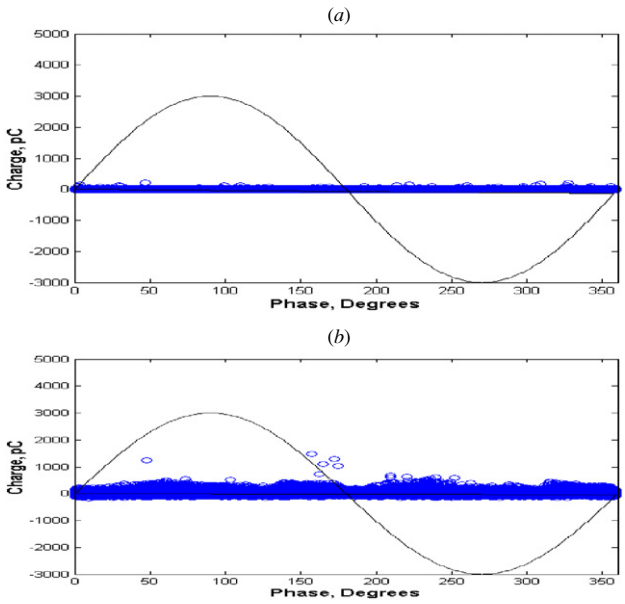

Figure 14. Cable 2: PD against phase (*a*) first measurement, 1421 cycles, (*b*) second measurement taken two months after the first, 2736 cycles.

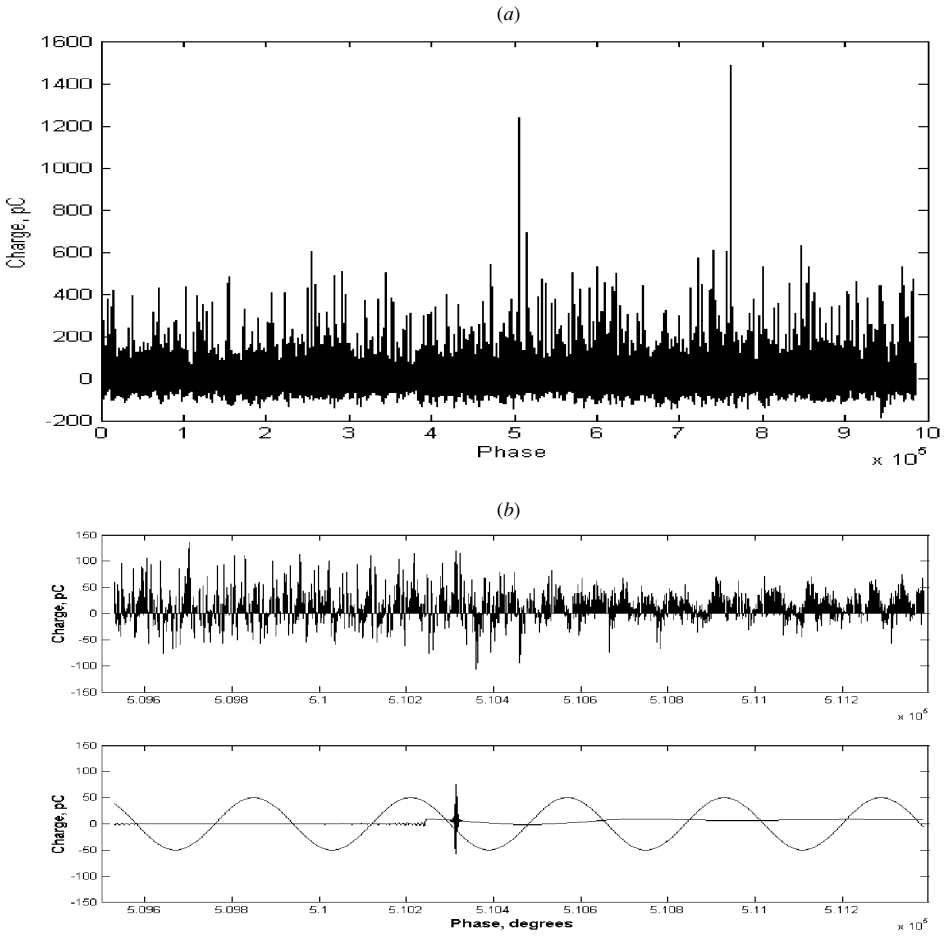

Figure 15. Cable 2: (*a*) second measurement raw data; (*b*) subset of denoised data, threshold equal to $\sigma/2$ and σ.

As can be seen from figures 12(*b*) and 13(*b*), especially for a threshold equal to the standard deviation, the denoised signal clearly demonstrates discharge activity in all quadrants of the applied cycle. Internal PDs are known to be found occurring during the first and third quadrants of the applied cycle. In addition as the cable has yet to fail this is unlikely to be internal PD. Another possible source of discharge activity could be a surface discharge in this case or a floating discharge activity or floating discharge event due to unconnected earth.

5.2. Cable 2: low levels of PD activity leading to eventual insulation failure

Figure 14 shows the two non-denoised phase plots of the measured PD signal, where the second measurement was again made two months after the first one. Unlike cable 1, lower discharge levels have been recorded and it might be assumed that cable 2 is less likely to fail in service. However, this cable failed 10 days after the second measurement had been made.

A window of the original time history of the second measurement performed on cable 2 is shown in figure 15 along with a section of denoised signal. Generally, denoising the two sets of measurement data yielded results with little evidence of

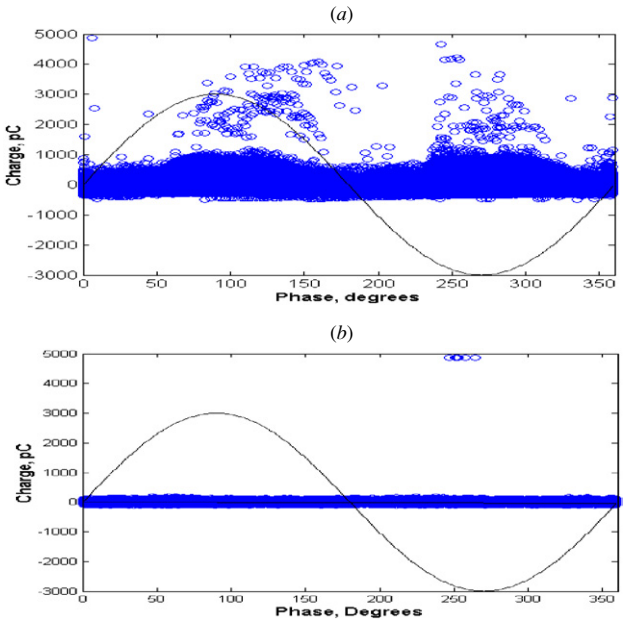

Figure 16. Cable 3: PD against phase (*a*) first measurement, 2568 cycles, (*b*) second measurement taken two months after the first, 2683 cycles.

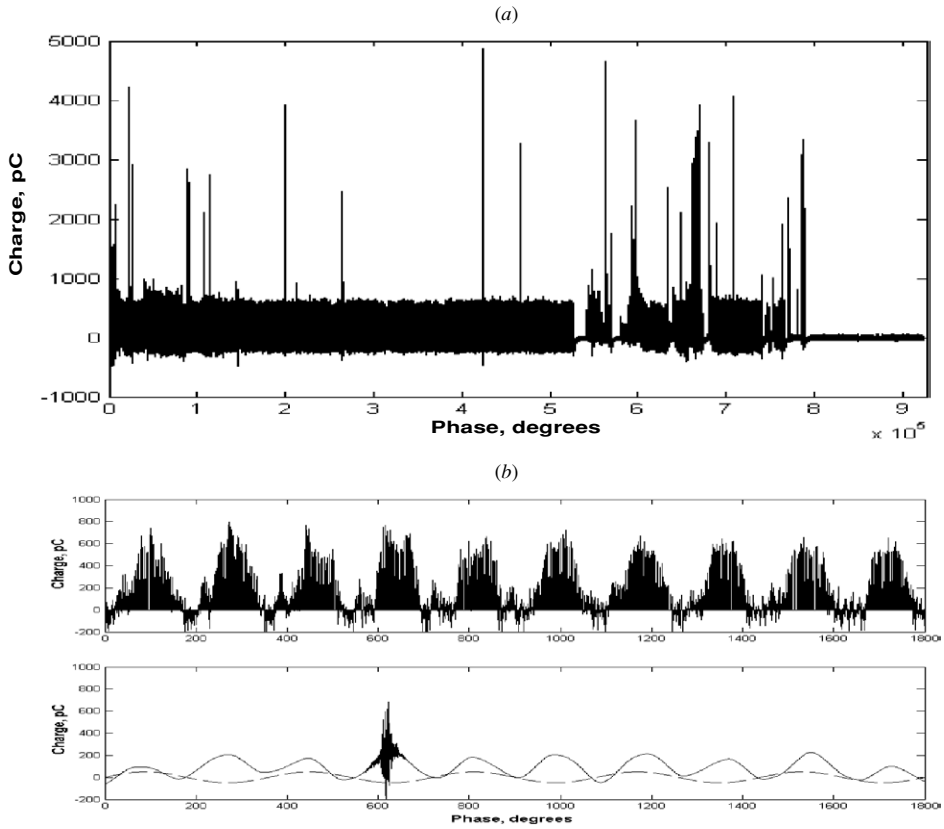

Figure 17. Cable 3: (*a*) first measurement raw data; (*b*) subset of denoised data, threshold equal to $\sigma/2$ and σ.

PD activity. However within the studied window, occasional events with a magnitude of 100 pC were detected. This could be indicative of a void-like discharge within the insulation of the cable, where the discharge event raises the void gas pressure effectively increasing the PD inception voltage. Over time the gas pressure reduces until the void can discharge again. Ultimately this action will lead to cable failure.

5.3. Cable 3: initial high levels of PD activity, followed by low levels and eventual insulation failure

Cable 3 initially had very high levels of PD activity (figure 16(*a*)), this activity had been substantially reduced in magnitude and number by the time the second measurement was made two months later (figure 16(*b*)). One month after the second measurement the cable failed.

As depicted in figure 17 buried in the noisy measurement is a 100 Hz sine waveform. What is more the second measurement showed no activity. The cable, nevertheless, eventually failed one month after the second measurement even though denoising produced results with little or no discharge activity.

All in all, the results demonstrate the strength of the algorithm to denoise experimental field data. As compared to conventional filtering this algorithm eliminates noise completely, without leaving behind any smoothed components, as supported by the denoising of cable 2 in which pure noise is completely eliminated. The adaptability of this algorithm is highlighted through the denoising of cable 3. In this case, the signal which is embedded in the noise is sinusoidal and it is denoised by exactly the same algorithm as the one used in the case of noisy PDs in cable 1. This adaptability is due to the vastness of the library from which the algorithm picks up basis functions to reconstruct the clean signal. The main important feature of this is that the denoising of any signal takes place on time scales that are well suited for online monitoring.

6. Conclusions

In this paper, a powerful denoising algorithm based on wavelet packets has been described and applied for the recovery of PDs in low SNR PD signals. The algorithm successfully recovered the PD signal in the majority of the cases considered, and was successful 60% of the time when the time bandwidth of the signal was around 1 ns, which constitutes a very extreme case in terms of real condition monitoring systems. It was revealed that the algorithm depends on the wavelets selected as well as on the standard deviation of the noise related to the PD time bandwidth.

The algorithm was subsequently applied to experimental field data obtained from cables in normal operation. In this application, the algorithm demonstrated its capability of denoising signals (PDs and sinusoids) of various shapes that are heavily corrupted by noise without assuming any *a priori* knowledge about the PD characteristics.

It is envisaged that the work that has been taking place, which shows the potential of the wavelet packet algorithm to effectively denoise highly corrupted signals, will be embedded in a wider scheme designed to check the integrity of cables in actual service and to help decide on any actions that need to be taken.

Acknowledgment

The authors would like to thank the Cyprus Research Foundation for supporting this work through the research project TEXNO/1104/10.

References

[1] Georghiou G E, Morrow R and Metaxas A C 1999 Theory of short-gap breakdown of needle point-plane gaps in air using finite-difference and finite-element methods *J. Phys. D: Appl. Phys.* **32** 1370
[2] Tian Y, Lewin P L, Davies A E, Swingler S G, Sutton S G and Hathaway G M 2002 Comparison of on-line partial discharge detection methods for HV cable joints *IEEE Trans. Dielectr. Electr. Insul.* **19** 604
[3] Morshuis P H F 1995 Partial discharge mechanisms in voids related to dielectric degradation *IEE Proc. Sci. Meas. Technol.* **142** 62
[4] Morshuis P H F and Niemeyer L 1996 Measurement and simulation of discharge induced ageing processes in voids *Proc. Conf. Electr. Insul. and Diel. Phenom. (San Francisco)* p 520
[5] Mayoux C and Laurent C 1995 Contribution of partial discharges to electrical breakdown of solid insulating materials *IEEE Trans. Dielectr. Electr. Insul.* **2** 641
[6] Avila S M and Horvath D 2000 Microscopic void detection as a prelude to predicting remaining life in electric cable insulation *NPIC & HMIT 2000 (Washington, DC)* p 1
[7] Georghiou G E, Lewin P L and Metaxas A C 2004 Guarding your assets: online monitoring tackles partial discharges *IEE Power Eng.* **18** 20
[8] Kreuger F H, Gulski E and Krivda A 1993 Classification of partial discharges *IEEE Trans. Electr. Insul.* **28** 917
[9] James R E and Phung B T 1995 Development of computer-based measurements and their application to PD pattern analysis *IEEE Trans. Dielectr. Electr. Insul.* **2** 838
[10] Heitz C 1999 A generalized model for partial discharge processes based on a stochastic process approach *J. Phys. D: Appl. Phys.* **32** 1012
[11] Alterburger R, Heitz C and Timmer J 2002 Analysis of phase-resolved discharge patterns of voids based on a stochastic process approach *J. Phys. D: Appl. Phys.* **35** 1149
[12] Wu K, Suzuoki Y and Dissado L A 2004 The contribution of discharge area variation to partial discharge patterns in disc-voids *J. Phys. D: Appl. Phys.* **35** 1815
[13] Kemp I J 1995 Partial discharge plant-monitoring technology: present and future developments *IEE Proc. Sci. Meas. Technol.* **142** 4
[14] Oyegoke B, Hyvönen P and Aro M 2001 Partial discharge measurement as diagnostic tool for power cable systems *Report* TKK-SJT-45, ISSN 1237-895X, Helsinki, Finland
[15] Wang P, Lewin P L and Sutton S J 2005 Calibration of capacitive couplers for online PD detection in HV cables *IEEE Electr. Insul. Mag.* **21** 28
[16] Boggs S and Densley J 2000 Fundamentals of partial discharge in the context of field cable testing *IEEE Electr. Insul. Mag.* **16** 13
[17] Wang P, Lewin P L, Tiam Y, Sutton S J and Swingler S G 2004 Application of wavelet based de-noising to online measurement of partial discharges *Int. Conf. Solid Diel. (Touluse, France)*
[18] Staszweski W J 1998 Structural and mechanical damage detection using wavelets *Shock Vib. Dig.* **30** 457
[19] Staszweski W J 1998 Wavelet based compression and feature selection for vibration analysis *J. Sound Vib.* **211** 735
[20] Shim I, Soragan J J and Siew W H 2000 Digital signal processing applied to the detection of partial discharge: an overview *IEEE Electr. Insul. Mag.* **16** 6
[21] Shim I, Soragan J J and Siew W H 2001 Detection of PD utilizing digital signal processing methods part 3: open loop noise reduction *IEEE Electr. Insul. Mag.* **17** 6
[22] Shim I, Soraghan J J and Shiew W H 2000 A noise reduction technique for on-line detection and location of PDs in high voltage cable networks *Meas. Sci. Technol.* **11** 1708
[23] Ma X, Zhou C and Kemp I J 2002 Automated wavelet selection and thresholding for PD detection *IEEE Electr. Insul. Mag.* **17** 37
[24] Ma X, Zhou C and Kemp I J 2002 Interpretation of wavelet analysis and its application in partial discharge detection *IEEE Trans. Dielectr. Electr. Insul.* **9** 446
[25] Satish L and Nazneen B 2003 Wavelet based denoising of partial discharge signals buried in excessive noise and interference *IEEE Trans. Dielectr. Electr. Insul.* **10** 354
[26] Zhou X, Zhou C and Kemp I J 2005 An improved methodology for application of wavelet transform to partial discharge measurement denoising *IEEE Trans. Dielectr. Electr. Insul.* **12** 586
[27] Lalitha E M and Satish L 2000 Wavelet analysis for classification of PD patterns *IEEE Trans. Dielectr. Electr. Insul.* **7** 40
[28] Kawada M, Tungkawananich M and Kawasaki Z-I 2000 Detection of wide band signals emitted from partial discharge occurring in GIS using wavelet transform *IEEE Trans. Power Dielectr.* **15** 467
[29] Boczar T and Zmarzly D 2004 Application of wavelet analysis to acoustic emission pulses generated by partial discharges I *IEEE Trans. Dielectr. Electr. Insul.* **11** 433
[30] Chang C S, Jin J, Kumar S, Su Q, Hoshino T, Hanai M and Kobayashi N 2005 Denoising of partial discharge signals in wavelet packets domain *IEE Proc. Sci. Meas. Technol.* **152** 129
[31] Chang C S, Jin J, Chang C, Hoshino T, Hanai M and Kobayashi N 2005 Separation of corona using wavelet packet and neural network for detection of partial discharge in gas-insulated substations *IEEE Trans. Power Deliv.* **20** 1363
[32] Hamid E Y and Kawasaki Z I 2002 Wavelet-based data compression of power system disturbances using the minimum description length criterion *IEEE Trans. Power Deliv.* **17** 460
[33] Chung J, Powers E J, Grady W M and Bhatt S C 2002 Power disturbance classifier using a rule-based method and wavelet packet based hidden Markov model *IEEE Trans. Power Deliv.* **17** 233
[34] Hamid E Y, Mardiana R and Kawasaki Z I 2002 Method for RMS and power measurements based on the wavelet packet transform *IEE Proc. Sci. Meas. Technol.* **149** 60
[35] Donoho D and Johnstone I 1994 Ideal denoising in an orthonormal basis chosen from a library of bases *C. R. Acad. Sci. Paris* I **329** 1317
[36] Donoho D and Johnstone I 1994 Ideal spatial adaptation via wavelet shrinkage *Biometrika* **81** 425
[37] Kyprianou A and Georgiou G H 2005 Wavelet packet denoising for on-line partial discharge detection in high voltage systems *Proc. 13th Med. Conf. Control & Autom. (Limassol, Cyprus)* pp 1184
[38] Mallat S 1989 Multi-resolution approximation and wavelet orthonormal bases of $L^2(R)$ *Trans. Am. Math. Soc.* **315** 69
[39] Mallat S 2001 *A Wavelet Tour of Signal Processing* (New York: Academic)
[40] Coifman R R, Meyer Y and Wickerhauser M V 1992 Wavelet analysis and signal processing *Wavelets and Their Applications (Boston, MA)* pp 153
[41] Donoho D L, Johnstone I M, Kerkyacharian G and Picard D 1995 Wavelet shrinkage: asymptotia *J. R. Stat. Soc.* B **57** 30
[42] Daubechies I 1992 *Ten Lectures on Wavelets* (Philadelphia, PA: SIAM)
[43] http://www-stat.stanford.edu/~wavelab/